

Article

# Screening of Additives to Ni-Based Methanation Catalyst for Enhanced Anti-Sintering Performance

Yuting Li <sup>1</sup>, Xiaoxia Han <sup>2</sup> , Chaofan Zhao <sup>2</sup>, Lin Yue <sup>2</sup>, Jinxian Zhao <sup>1</sup> and Jun Ren <sup>1,\*</sup> 

<sup>1</sup> Key Laboratory of Coal Science and Technology, Taiyuan University of Technology, Ministry of Education and Shanxi Province, No. 79 Yingze West Street, Taiyuan 030024, China; liyuting0482@163.com (Y.L.); zhaojinxian@tyut.edu.cn (J.Z.)

<sup>2</sup> College of Electrical and Power Engineering, Taiyuan University of Technology, No. 79 Yingze West Street, Taiyuan 030024, China; hanxiaoxia@tyut.edu.cn (X.H.); fantasyzhao@foxmail.com (C.Z.); yuelin0282@link.tyut.edu.cn (L.Y.)

\* Correspondence: renjun@tyut.edu.cn; Tel.: +86-351-6018598

Received: 20 April 2019; Accepted: 24 May 2019; Published: 28 May 2019



**Abstract:** The resistance to sintering of Ni/Al<sub>2</sub>O<sub>3</sub> catalysts with different additives for methanation reaction was modeled and predicted by data mining. In the screening, the resistance to sintering of Na, Ca, Ce, Mg, La, Cu, Zn, Zr, In, Mo, and Ti promoted Ni/Al<sub>2</sub>O<sub>3</sub> catalyst were measured in terms of the increased rate of the size of the metallic nickel particles. The resistance to sintering of catalysts, described by the increased rate of Ni particle size as well as basic physicochemical properties of the 11 selected elements, was adopted for optimization model construction by data mining. Through regression model prediction and experimental verification, Cs was found to be an additive, and promotes the resistance to sintering mostly for Ni/Al<sub>2</sub>O<sub>3</sub> catalysts. This result provides further evidence that data mining techniques can be employed as a highly efficient tool for the discovery of new catalysts in comparison with the traditional experimental method.

**Keywords:** data mining; methanation; Ni/Al<sub>2</sub>O<sub>3</sub> catalyst; additives; anti-sintering

## 1. Introduction

Natural gas is a clean fossil fuel, and the global consumption of natural gas has increased steadily in the last decade [1–6]. Nevertheless, reserves of natural gas are expected to be depleted in the next few decades and its prices are continuously rising [7–10]. In this respect, synthetic natural gas (SNG) production from syngas from coal or renewable biomass has received significant attention in some countries. The conventional route for SNG procedure is in accordance with the gasification and methanation of coal to synthetic gas (CO+H<sub>2</sub>) [4,11,12]. More recently, at least 15 coal-to-gas plants are planned in the United States, and more than 20 coal-to-gas plants are under construction and planned in China [13]. CO reaction (CO + 3H<sub>2</sub> → CH<sub>4</sub> + H<sub>2</sub>O, ΔH<sub>298K</sub> = −206.1 kJ mol<sup>−1</sup>), as one of the fundamental steps in making coal-formed gas process, has raised broad interest after Sabatier and Senderens originally discovered it in 1902 [14]. This can to a large extent be attributed to its broad utility in chemical production, e.g. elimination of micro amounts of CO from H<sub>2</sub>-rich feed gas, purification of reforming gas for fuel-cell manufacture, technologies in respect of Fischer–Tropsch synthesis production, among others [15–18]. Hence, exploiting a new and high-efficiency catalyst for methanation is nowadays a matter of great concern.

Normally, Ni supported on Al<sub>2</sub>O<sub>3</sub> is one of the most widely studied catalysts in methanation reactions for the production of SNG as a result of its lower price, higher catalytic activity, and the better selectivity for the methane product [19–23]. Al<sub>2</sub>O<sub>3</sub>, especially the γ-modification with larger specific surface area and mechanical strength, developed pore structure, and greater acid and alkali

resistance on the surface, strongly affects the catalytic performance, which increases activity and stability for methanation [24,25]. However, methanation, as a key step of SNG production, is a highly exothermic reaction. For each 1% CO and each 1% CO<sub>2</sub>, the representative methanation gas component temperature rise in ammonia plants is 74 and 60 °C, separately [26]. In the high-temperature reaction environment, the Ni-based methanation catalyst is prone to sintering, resulting in the accelerated migration and aggregation of the nickel microcrystalline particles, and the decrease of the nickel dispersion and the effective specific surface area [27,28]. Al<sub>2</sub>O<sub>3</sub> support also suffers the disadvantage of poor thermal stability. Thus, the catalytic activity is reduced. Therefore, solving the catalyst sintering problem is the biggest challenge for the methanation process.

Many efforts have been devoted to further increasing the performance of resistance to sintering of Ni/Al<sub>2</sub>O<sub>3</sub> catalyst. The sintering rate of the catalyst is related to the size and distribution of the nickel crystallites, the structure, morphology and transition state of the support [26]. Adding additives is one of the most effective means to improve the anti-sintering performance of the catalyst. For example, adding ZrO<sub>2</sub> can sequester NiO and  $\gamma$ -Al<sub>2</sub>O<sub>3</sub> and weaken their interactions, which play the role of limiting the aggregation of  $\gamma$ -Al<sub>2</sub>O<sub>3</sub> [17]. The addition of Rh and Ru was reported to improve the heat stability of nickel loading on alumina [29,30]. Adding La<sub>2</sub>O<sub>3</sub> [1], MgO [31] can form LaAlO<sub>3</sub> and MgAl<sub>2</sub>O<sub>4</sub> surface layers and prevent their activity component Ni<sup>2+</sup> diffused into the Al<sub>2</sub>O<sub>3</sub> bulk phase to form NiAl<sub>2</sub>O<sub>4</sub>, slowing down the catalyst sintering rate. CeO<sub>2</sub> was added to inhibit the migration of Ni atoms on the surface of Al<sub>2</sub>O<sub>3</sub> and improve the dispersion of nickel particles owing to the strong metal–support interaction (SMSI) [32]. Recently, Ma et al [33] and Bao and coworkers [34] reported that encapsulating Ni particles with graphene or hexagonal boron nitride shells could enhance the anti-sintering ability of Ni-based methanation catalysts.

Although a lot of research efforts have been made towards searching for new promoters to improve the resistance to sintering of Ni/Al<sub>2</sub>O<sub>3</sub> catalysts for methanation [31–37], it is difficult to understand the intrinsic contribution of various promoters because of the complexity of the catalytic mechanism. As a result, the exploration of new additives for methanation catalysts has mainly been dependent on trial and error methods until now.

In contrast with the traditional catalyst development, whereby researchers obtain all the handled experimental results and provide guidance for the subsequent studies, data mining as a new approach does not require any starting hypotheses, since it can be readily applied to any non-linear catalytic phenomena and global search potential correlations and modes between the input variables (catalysts component, preparation conditions, and reaction parameters) and output variables (catalysts characterization and performance) through massive amounts of raw information [38]. In our previous work, data mining techniques was used to screen potential additives of Ni/Al<sub>2</sub>O<sub>3</sub> catalyst for improving the catalytic activity [39]. We constructed a regression model through data mining and it forecast that as a potential auxiliary agent, Re improves the catalytic activity. There is an acceptable agreement between the predicted and experimental results. More specifically, it demonstrated that Re can be considered to be the most effective of all additives. These powerful computational techniques avoid the blind search process and complex interactions within the catalyst and could expedite the design of new catalyst systems.

Anti-sintering performance is another important indicator of methanation catalysts [40,41]. It is of great significance to predict and screen new additives based on existing experimental data. And as such the aim was to select element additives, which can retain high resistance to sintering at long-term high temperatures. In this paper, data mining was used to build an optimization model and to forecast the resistance to sintering of Ni/Al<sub>2</sub>O<sub>3</sub> catalysts with different additives, thus screening the optimal additives.

## 2. Results and Discussion

Data mining is an emerging concept, mainly referring to the process of knowledge discovery in databases. It constantly explores how to extract knowledge that is difficult to obtain through theoretical

calculations from some massive and seemingly disorganized observation data. This knowledge often has the following characteristics: it is previously unknown, effective and practical. It is then used to analyze practical problems and make effective predictions for complex, fuzzy, and jagged datasets. Normal process of the data mining is shown in Figure 1. The general procedure of the data mining is summarized, including a) data collection, b) data cleaning, c) data transformation, d) data loading, e) data analysis and f) result report. Owing to the diversity of data sources, aggregation is required prior to loading the data [41]. The specific explanation for using data-mining screen additives of Ni/Al<sub>2</sub>O<sub>3</sub> catalyst is as follows:

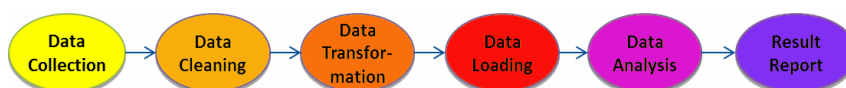


Figure 1. Normal process of data mining.

### 2.1. Data Collection

This design aims to model the relationship between the additives of Ni/Al<sub>2</sub>O<sub>3</sub> catalyst and its anti-sintering performance through data-mining technology. The optimal additive is then predicted and screened. Therefore, when modeling, different additive elements are taken as input, and their corresponding anti-sintering properties are taken as output. The basic process and data to be collected is shown in Figure 2.



Figure 2. Input, output and process of modeling.

#### 2.1.1. Input Data

Based on previous research results, 63 elements except for gases, poisons, radioactive ones were selected as candidate additives for Ni/Al<sub>2</sub>O<sub>3</sub> catalyst. The inter-relationship between the type of the element additives and the resistance to sintering of Ni/Al<sub>2</sub>O<sub>3</sub> catalysts is then established. Here, the additive element cannot be applied straightforwardly as input variables and need to be transformed into a series of representative data. Physicochemical properties of elements affect the catalytic performance, i.e. specific surface area, metal dispersion degree, electron configuration, morphology features, and heat stability. These properties, in sequence, identify the catalytic performance [42–45]. Moreover, the physicochemical properties of additive elements were selected as explanatory variables that describe each element and were used for the prediction of the catalytic performance in the process of building the regression model.

In this study, 16 physicochemical properties were utilized as proper descriptors for each element, illustrated by Table 1. In the field of data-mining technology, these properties were recorded in the “data.csv” file, as explained in Table 2, where only a portion of the file is displayed. The properties are stored in the 1–16th columns. Correlated symbols are stored in the 17th column, simultaneously.

Table 1. Physicochemical property for featuring each element.

Property	Unit	Property	Unit
1st ionization energy (I1)	eV	2nd ionization energy (2I)	eV
electric dipole polarizability (ED)	Å <sup>3</sup>	electronegativity (EN)	-
melting point (MP)	K	boiling point (BP)	K
oxide formation enthalpy(FE)	kJ/mol	specific heat capacity (HC)	J/g/K
heat of fusion (HF)	kJ/mol	heat of vapor vaporization (HV)	kJ/mol
thermal conductivity (TC)	W/mK	density (DS)	g/cm <sup>3</sup>
covalent radius (CR)	pm	ionic radius (IR)	pm
atomic weight (AW)	g/mol	valence of ion (VA)	-

**Table 2.** Data file for data-mining techniques.

	FE	II	...	VA	Symbol
1	416	4.958	...	1	Na
2	601.8	7.377	...	2	Ca
⋮	⋮	⋮	⋮	⋮	⋮
63	217.6	7.156	...	3	Pb

16 physicochemical properties as the explanatory variables were reduced by principal component analysis (PCA), which is clarified in Section 2.3.

### 2.1.2. Output Data

For the purpose of ensuring the accuracy of regression model, data of 63 elements that enable the whole periodic table to be represented were available for K-means element cluster analysis [46,47]. Subsequently, one or two characteristic elements were chosen for each cluster. A pool of 11 elements (Na, Ca, Ce, Mg, La, Cu, Zn, Zr, In, Mo, and Ti) was chosen for the corresponding experiment.

The obtained experimental data were shown in Table 3. Bare is the Ni/Al<sub>2</sub>O<sub>3</sub> catalyst. The crystallite sizes of the Ni, before and after catalyst evaluation, were marked as d and d'. The variation of crystallite sizes of the Ni were marked as d<sub>Δ</sub>.

**Table 3.** Experimental result of anti-sintering for data mining.

	Additive	Crystallite Sizes of the Ni (nm)			Increase Rate
		d	d'	d <sub>Δ</sub>	
1	In	28.1	36.2	8.1	0.288
2	Na	15.8	22.9	7.1	0.449
3	Ti	51.3	76.0	24.7	0.481
4	La	14.2	21.7	7.5	0.528
5	Zr	14.8	22.9	8.1	0.547
6	Bare	14.1	22.2	8.1	0.574
7	Cu	14.4	22.7	8.3	0.576
8	Ce	16.9	27.0	10.1	0.598
9	Mg	16.4	28.0	11.6	0.707
10	Mo	15.0	26.1	11.1	0.740
11	Ca	16.0	28.1	12.1	0.756
12	Zn	14.9	29.4	14.5	0.973

Sintering leads to an increase in Ni crystallites, which is one of the main reasons for catalyst deactivation. The increase rate of crystallite size of the Ni was selected as output variables and used for data analysis. The lower the increase rate, the better anti-sintering performance.

### 2.2. Data Cleaning

Data cleaning can be defined as a process of which damages or errors are detected and corrected (or eliminated) in data representation among data sources. The ultimate goal is to gain high-quality data that is elementary for accurate data analysis [48]. The datasets assembled in our work is intact and reliable, and there is no need to clean.

### 2.3. Data Transformation

The use of 16 physicochemical properties to characterize each additive element means that the input variable is transformed into a set of 16-dimensional data. At this point, the input variable has a larger dimension. High dimensionality makes analysis extremely difficult and unfavorable for modeling; additionally, the required computing time would become much longer [49]. Hence, reducing the amount of input variables is crucial through data transformation.

Dimension reduction is of great importance; on the one hand, high-dimensional data cannot be directly applied in some specific algorithm, dimension reduction can solve the “dimension disaster” (that is involved in vector calculation problems, computation exponentially multiply with the increase of digits), reduce the complexity of data, ensuring some algorithms can be used normally; On the other hand, high-dimensional data often contain a lot of noise and redundancy. Dimensional reduction can refine the data structures of interest in high-dimensional data and present them in low-dimensional space in order to better understand the data.

PCA is used in almost all scientific disciplines in reducing dimensionality [50]. PCA is based on the location distribution of the sample point in the multidimensional pattern space, the maximum direction of variance, which is the maximum direction of the change of the sample point in the space, as the discriminant vector to realize the feature extraction and data compression of the data. From the point of view of probability and statistics, the greater the variance of a random variable, the more information the random variable contains. If the variance of a variable is zero, this variable is a constant value and it does not contain any information. The so-called principal components are new variables obtained by a linear combination (or mapping) of several variables of the original data. The first principal component might have the maximum variance; each principal component is linearly independent, that is, orthogonal. From the first principal component, the principal components are arranged in the order of variance (i.e. the corresponding eigenvalues are arranged in the order of size). The later principal components are considered to be included in the noise and redundancy, and these variables are not introduced into the model in the analysis. Thus PCA can conduce to extracting most of the signal into the first few principal components, reducing the principal component of the analysis to achieve the purpose of reducing the dimension.

The number of input variables (16 physicochemical properties) was lessened by means of PCA. As can be seen in Figure 3, the cumulative contribution ratio versus the amount of principal component is presented.

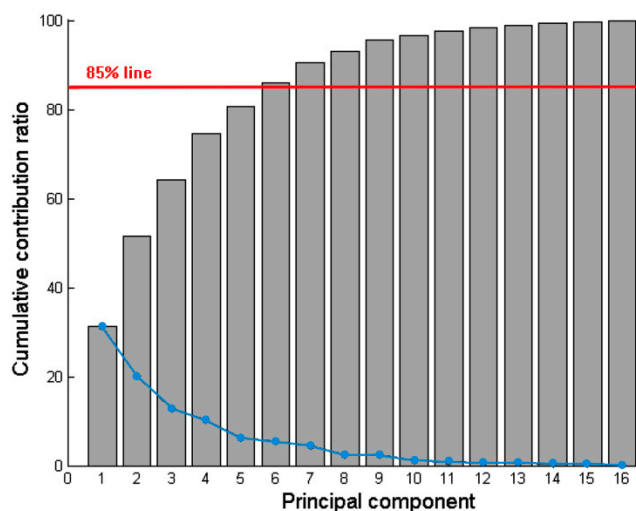


**Figure 3.** Scree plot of the cumulative contribution ratio versus principal components of the physicochemical properties.

The scree plot indicates that the cumulative contribution ratio of 6 principal components involves more than 85% information. As a matter of fact, 6 principal components are adequate to generalize the characteristic of 16 physicochemical properties. Thereby, 16 physicochemical properties were converted to 6 principal components, which were used for data mining. The details were recorded in the “pcdata.csv” file as shown in Table 4.

Table 4. Principal component.

	Symbol	PC1	PC2	PC3	PC4	PC5	PC6
1	Na	-4.4937	-2.3331	-0.3341	1.6384	-0.5100	0.5386
2	Ca	-2.3613	-0.5930	-0.2064	0.2247	0.6403	-0.5807
3	Ce	-0.4507	2.3991	0.2552	0.3157	-0.1669	-0.2053
4	Mg	-1.6915	-2.1294	0.5409	-0.3025	0.3747	-0.8766
5	La	-0.7296	2.5065	0.3964	0.4895	-0.2748	-0.0154
6	Zr	0.4382	1.0243	1.2377	0.0225	-0.0842	-0.3463
7	Cu	0.5306	-2.7485	-1.8363	0.3687	0.4199	-0.7745
8	Zn	-0.5839	-2.1809	-0.4995	-1.5155	0.3046	-0.8257
9	In	-0.5671	-0.1366	-0.1965	-0.7385	-0.1178	-0.7170
10	Mo	2.9809	-0.0167	0.1473	1.1944	0.0759	0.1035
11	Ti	-0.0041	0.7963	1.6307	1.5408	7.1646	0.7350
12	Cs	-5.5148	2.1166	-2.1336	0.3439	0.2223	1.0677
13	Pb	0.0123	-0.1370	-2.3945	-1.8833	-0.0560	-0.1917
14	Bi	-0.1575	0.2925	-1.2227	-2.1246	-0.2919	-0.2747
15	Li	-5.3394	-4.9617	1.5072	4.4598	-2.1287	1.6791
16	Be	-0.0422	-3.7374	1.3584	0.9780	0.0000	-0.8547
17	B	1.8890	-2.1963	2.6368	1.1828	-0.3254	0.2201
18	Al	-0.4859	-1.5670	1.4001	0.5802	-0.1453	-1.1017
19	Si	1.3901	-1.8215	1.8616	0.0100	0.1982	-0.4558
20	P	0.1109	-1.6922	3.9914	-2.8601	-0.6084	-1.9119
21	K	-5.2054	-0.1698	-1.0614	1.0598	0.1477	0.6275
22	Sc	-0.3441	0.4999	1.9521	0.3799	-0.0789	-0.4072
23	V	-0.0921	-0.3732	1.2543	-0.0726	-0.1303	-0.2292
24	Mn	-0.0243	-1.0383	0.6824	-0.2757	0.0628	-0.4408
25	Fe	0.7548	-1.1968	0.1286	0.1516	0.1281	-0.3575
26	Co	0.8136	-1.4482	-0.6134	0.2281	0.2527	-0.2292
27	Ni	0.8075	-1.4076	-0.3220	0.2367	0.1353	-0.2136
28	Ga	-0.5398	-0.6326	0.7324	-0.5734	-0.1867	-0.8265
29	Ge	1.1991	-1.0044	0.9964	-0.8346	0.1748	-0.4919
30	As	0.9978	-2.7580	2.3675	-4.7562	0.0112	5.6521
31	Rb	-5.1896	0.9599	-1.6261	0.4956	0.2165	0.7728
32	Sr	-2.6362	0.9411	-0.3388	-0.2900	0.5101	-0.0959
33	Y	-0.2723	1.5312	1.2343	0.5041	-0.0971	-0.1741
34	Ru	2.6622	-0.5648	-0.8152	0.9724	0.1674	0.1244
35	Nb	2.1728	1.1007	1.0659	1.6163	-0.2420	0.2596
36	Rh	2.3402	-0.8977	-0.8947	0.5321	0.1227	-0.0666
37	Pd	1.3995	-1.2676	-1.3862	-0.2708	0.1700	0.0564
38	Ag	-0.2682	-2.4074	-3.6047	0.0505	0.4128	-0.3322
39	Cd	-0.7424	-1.4188	-1.2913	-1.8597	0.3148	-0.6027
40	Sn	0.6506	-0.3180	0.1437	-1.1355	0.0984	-0.9817
41	Sb	0.1471	-0.7792	0.2540	-2.0601	0.0053	-0.5371
42	Ba	-2.9022	2.0680	-1.0525	-0.1713	0.3115	0.2947
43	Cr	0.4685	-1.0551	0.2006	0.6326	0.1772	-0.2196
44	Pr	-0.5280	2.2808	0.2327	0.1221	-0.1295	-0.2281
45	Nd	-0.8871	2.3965	0.4200	0.0970	-0.3468	-0.0491
46	Sm	-1.3286	2.0645	0.4123	-0.6867	-0.3939	-0.1523
47	Eu	-1.5234	1.8859	0.4615	-0.8284	-0.1108	-0.1924
48	Gd	-0.0690	2.0926	0.4568	0.2059	-0.3961	0.0243
49	Tb	0.0368	2.5625	0.8608	0.0744	-0.4979	-0.1087
50	Dy	-0.3856	2.1112	0.4324	-0.2671	-0.4420	0.0111
51	Ho	-0.2105	2.0891	0.4164	-0.2174	-0.4525	0.0306
52	Er	0.0875	2.1022	0.4785	-0.0846	-0.4758	0.1911
53	Tm	-0.2964	1.8734	0.4289	-0.6181	-0.4749	0.0745
54	Yb	-1.1545	1.6328	0.4297	-1.1359	-0.2951	-0.3353
55	Lu	0.3369	2.2590	0.3557	0.3901	-0.5661	0.3121
56	Hf	2.3448	1.8948	0.1696	1.0018	-0.4667	0.4073
57	Ta	3.7629	1.7138	0.2209	1.6872	-0.6980	0.8046
58	Ir	4.2483	-0.3053	-2.0454	0.5417	-0.2065	0.4819
59	Pt	3.2775	-0.6054	-2.2724	-0.0009	-0.2082	0.4988
60	Au	2.1345	-2.1964	-3.9288	-0.5559	0.0923	-0.0104
61	Tl	-1.0802	0.8609	-2.4039	-1.3550	-0.4237	0.0548
62	W	5.2568	0.5402	-1.0652	1.8146	-0.3212	0.7266
63	Re	4.8499	1.4997	-0.2068	1.3307	-0.5620	0.6653

#### 2.4. Data Loading

Data mining (Supplementary Materials) was conducted in our work using the statistic language R. The datasets were loaded on R and the main functions used were:

**prcomp** for PCA,

**Kmeans** for element k-means clustering analysis, and

**bgp** as the installation package developed by Gramacy for modeling [51,52].

#### 2.5. Data Analysis

As mentioned earlier, the models for screening potential additives was determined using the 22 data sets comprised the input data, that is, six principal components of 11 elements, and the target values, containing resistance to sintering feature. However, a small sample of data makes processing and modeling tough. Prior modeling with small data sets, an adaptable data analysis methodology was chosen properly to overcome this limitation.

The successful application of various widespread modeling and optimizing approaches has been already investigated and reported by many researchers in the design of catalysts [53–57]. So far, artificial neural networks (ANN) and support vector machines (SVM) are the most universal because of their wide range of suitability, particularly in nonlinear catalytic phenomena for finding correlations. However, the accuracy of ANN and SVM methods utilized for modeling and predicting was not sufficient in this research with respect to the viewpoint of regression models.

- As original methods, ANN and SVM are suitable for processing large datasets; the model should be therefore constructed using a mass of validation data to ensure its applicability and reliability. Considering the situation above, those two methods are not appropriate for data analysis of small sample datasets.
- Input of several key parameters utilized frequently in ANN and SVM can have a large impact on the feasibility of the model; for instance, the type of kernel functions adopted by an SVM, or the structure design parameter of a neural network. Parameter optimisation is significant and become more difficult on the basis of small sample datasets.
- There are no indicators in ANN and SVM for further improving accuracy of the regression model.

To tackle these obstacles, a Gaussian process regression (GPR) methodology was applied to promote the catalytic performance of the resistance to sintering by establishing a regression model in accordance with the physicochemical properties of each selected element. The major advantage for exploiting this probabilistic nonparametric modeling method into the resistance to sintering of the catalysts optimization is that, accuracy of the modeling prediction and applicability of analyzing high-dimensional, nonlinear, small sample datasets [58,59].

$$y = \sum_{i=1}^9 w_i \exp \left[ -\frac{1}{2\sigma_i} (x - c_i)^2 \right], \quad (1)$$

where  $w_i$  is the weight,  $c_i$  the center vector, and  $\sigma_i$  the radius. Thus, the output  $y$  is calculated from the input vector  $x$ .

It is difficult to find appropriate parameters when modeling with small datasets. In the present study, a nonparametric algorithm is applied to the GPR model, that is, the estimated parameters are not necessary. The weights of GPR, as an a posteriori probability, were determined. Moreover, a unique radius parameter in each dimension was employed in the **bgp** function. Both improvements made for better performance of the GPR.

In particular, expected improvement (EI) function was introduced into the GPR and the indicator EI was produced [60]. EI that serves as discrimination criteria of the new potential optimal solution manifests itself in possibly increasing the predictability and feasibility of the GPR model since the

experimental results were applied to the modeling. Therefore, imperative supplementary tests are forecast by the index EI. If the largest EI is approaching zero, then the optimization process can be completed owing to no further expected improvement which is found by performing supplementary tests. Figure 4 displays a flowsheet for the process of modeling and anticipating by data mining techniques in this part of work.

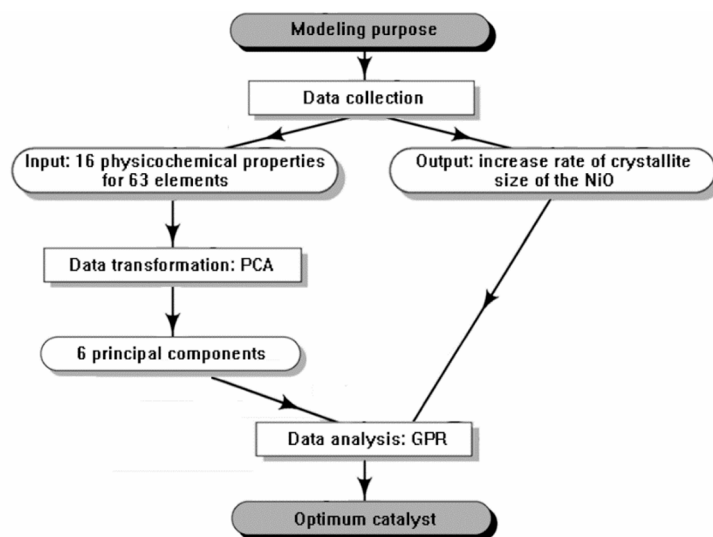


**Figure 4.** Flowsheet for modeling and anticipating by data-mining techniques.

## 2.6. Result Report

For developing the GPR model, as in Table 4, model input data were PC1–PC6 for Na through Ti. Meanwhile, the increase rate of Na through Ti has been utilized as model outputs, summarized in Table 3. Thereafter, Table 4 clearly gives PC1–PC6 for Cs through Re, used for predicting the outcome in GPR model. Figure 5 respectively illustrates the increase rate of Cs through Re, which has been already predicted by aforementioned procedure, and ranked elements in accordance with the EI.

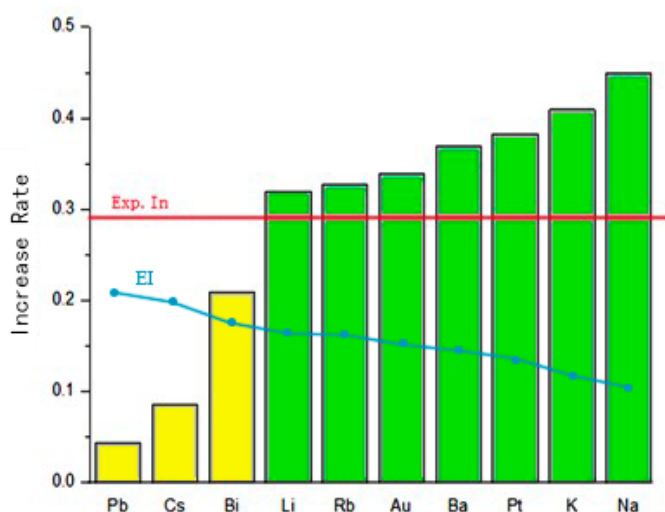


**Figure 5.** Prediction of the 1st Gaussian process regression (GPR) model selected by the expected improvement (EI) ranking.

From the perspective of additional experiments, effectively additive elements of Pb, Cs, and Bi were explored, according to their high resistance to sintering of the catalysts and high EI. The predicted increased rate (*Means*) and the 90% confidence interval ( $q1, q2$ ) are listed in Table 5. Thereby,

experiments with respect to the anti-sintering of Pb, Cs, and Bi, which promoted Ni/Al<sub>2</sub>O<sub>3</sub> catalytic performance, were executed. More detailed data correlated with resistance to sintering are revealed in Table 6 and experimentally determined.

**Table 5.** Prediction by the first regression model for further screening.

Rank	Symbol	EI	Means	q1	q2
1	Pb	0.2125	0.0427	0.0321	0.0747
2	Cs	0.1954	0.0819	0.0467	0.1024
3	Bi	0.1658	0.2176	0.1378	0.3375

**Table 6.** Experimental result of anti-sintering for verifying.

	Additive	Crystallite Sizes of the Ni (nm)			Increase Rate
		d <sub>1</sub>	d <sub>2</sub>	d <sub>Δ</sub>	
1	Cs	15.7	22.4	6.4	0.408
2	Pb	16.0	23.9	7.9	0.494
3	Bi	23.0	54.2	31.2	1.357

According to these results, it is apparent that three additive elements, namely, the Pb, Cs, and Bi, with resistance to sintering superior than one of Ni-In/Al<sub>2</sub>O<sub>3</sub> catalysts, which were estimated to be candidates. However, this prediction was incorrect. The increase rate for Ni-Pb/Al<sub>2</sub>O<sub>3</sub>, Ni-Cs/Al<sub>2</sub>O<sub>3</sub>, and Ni-Bi/Al<sub>2</sub>O<sub>3</sub> catalysts are higher than that of Ni-In/Al<sub>2</sub>O<sub>3</sub> catalysts. Thereafter, additional experiments were carried out utilizing Pb, Cs, as well as Bi element for building the second regression model by GPR. In this context, as depicted by Figure 6, elements were ranked with respect to the EI. Through the prediction of the second regression model, it is found that among the remaining elements, adding Li has the best anti-sintering performance, and the detailed data are shown in Table 7. However, the experimental results reveal that the effect of adding Li is not as good as that of adding Cs; furthermore, its EI value is quite low. Consequently, the screening process was eventually finished.

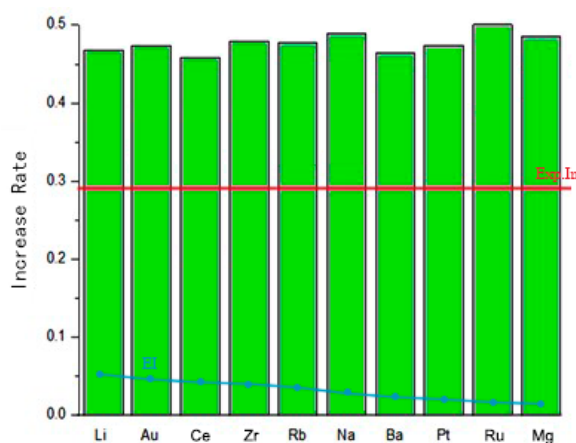


**Figure 6.** Prediction of the 2nd GPR model selected by the EI ranking.

**Table 7.** Prediction by the second regression model for further screening.

Rank	Symbol	EI	Means	q1	q2
1	Li	0.05124	0.4279	0.3165	0.5762

It is noticeable that, as one of the Ni/Al<sub>2</sub>O<sub>3</sub> catalytic promoters, Cs addition possessed exceptional performance, which was determined by the predicted model outputs and its corresponding experimental

values. Although the increase rate of Ni-Cs/Al<sub>2</sub>O<sub>3</sub> catalysts are higher than that of Ni-In/Al<sub>2</sub>O<sub>3</sub> catalysts, its crystallite sizes of the Ni, before and after catalyst evaluation, are less than those of Ni-In/Al<sub>2</sub>O<sub>3</sub> catalysts. Apart from those mentioned above, more significantly, it has the minimal variation of crystallite sizes of the Ni.

### 2.7. Effect of Physicochemical Properties on Catalytic Anti-Sintering

The superiority of regression model by GPR in finding an anti-sintering Ni-Cs/Al<sub>2</sub>O<sub>3</sub> catalyst is verified by the obtained results. It obviously shows that the proposed model can quickly search for potential optima with respect to improvement of regression accuracy and suggestion of necessary additional experiments. Another major concern is whether underlying non-linear correlations or patterns are existed in the regression model, which is determined by GPR, between the physicochemical properties and catalytic performance of resistance to sintering. Based on the method of virtual elements, the effect of physicochemical properties of each element on resistance to sintering was calculated.

As indicated in Table 2, one of the physicochemical properties of Cs was selected to change from the minimum to the maximum of the performance of 63 elements. Accordingly, the six principal components and the growth rate predicted by GPR model were also changed. Consequently, the effect of the physicochemical property can be estimated. Difference of the predicted increased rate chosen here, that is, corresponding to the difference between 20% and 100% of the normalized physicochemical property, represented the influence of different physicochemical properties on the anti-sintering performance of the catalyst, by reason that the effects were monotonous. As can be seen in Figure 7, the effects of size factors, for instance, IR (ionic radii), DS (density), and AW (atomic weight) are large in the sintering resistance, while the effects of thermal properties such as HV (heat of vaporization), MP (melting point), BP (boiling point) are small. Particularly, IR (ionic radii) is an important factor to limit Ni sintering. The difference of the predicted increased rate obtained by calculation, whose absolute value greater than 0.6, is the largest of all values. In this manner, the influence of each property on the catalytic anti-sintering clearly showed that some properties are influential and others are not. Whereas how those different properties affect the anti-sintering performance is not revealed immediately, this should be clarified in further research.

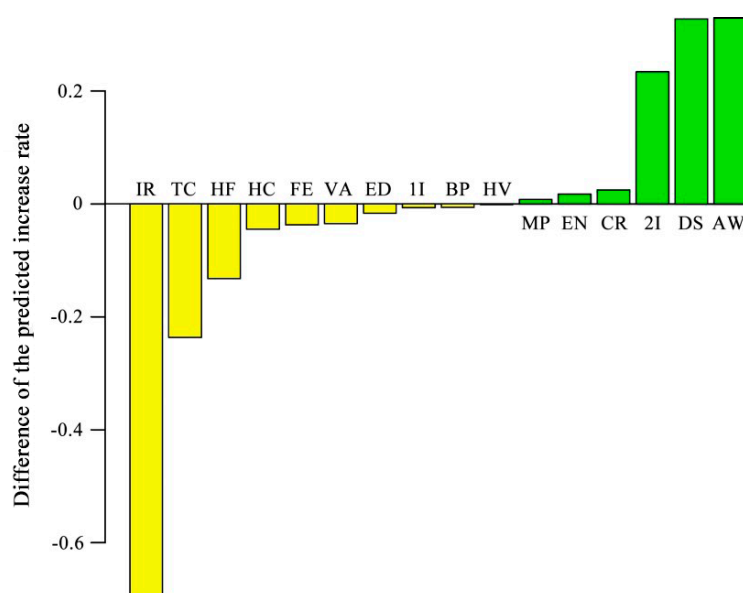


**Figure 7.** Influence of physicochemical properties on the anti-sintering of the Ni-Cs/Al<sub>2</sub>O<sub>3</sub> catalyst.

### 3. Experimental Section

#### 3.1. Materials

All the reagents were of analytical grade and used as received, which are embodied below:  $\text{NaNO}_3$ ,  $\text{Ca}(\text{NO}_3)_2 \cdot 4\text{H}_2\text{O}$ ,  $\text{Ce}(\text{NO}_3)_3 \cdot 6\text{H}_2\text{O}$ ,  $\text{Mg}(\text{NO}_3)_2 \cdot 6\text{H}_2\text{O}$ ,  $\text{La}(\text{NO}_3)_3 \cdot 6\text{H}_2\text{O}$ ,  $\text{Cu}(\text{NO}_3)_2 \cdot 3\text{H}_2\text{O}$ ,  $\text{Zr}(\text{NO}_3)_4 \cdot 5\text{H}_2\text{O}$ ,  $\text{Zn}(\text{NO}_3)_2 \cdot 6\text{H}_2\text{O}$ ,  $\text{In}(\text{NO}_3)_3 \cdot 4.5\text{H}_2\text{O}$ ,  $\text{H}_{24}\text{Mo}_7\text{N}_6\text{O}_{24} \cdot 4\text{H}_2\text{O}$ ,  $\text{C}_{16}\text{H}_{36}\text{O}_4\text{Ti}$ ,  $\text{Cs}_2\text{CO}_3$ ,  $\text{Bi}(\text{NO}_3)_3 \cdot 5\text{H}_2\text{O}$ ,  $\text{PbC}_4\text{H}_6\text{O}_4 \cdot 3\text{H}_2\text{O}$ ,  $\text{Ni}(\text{NO}_3)_2 \cdot 6\text{H}_2\text{O}$ , and deionized water. After calcining in air at  $550\text{ }^\circ\text{C}$  for 6 h, commercial  $\gamma\text{-Al}_2\text{O}_3$  can be used.

#### 3.2. Catalyst Preparation

Presently, a total of fourteen elements (Na, Ca, Ce, Mg, La, Cu, Zn, Zr, In, Mo, Ti, Cs, Bi, and Pb) were selected as candidates in the experiment for the additives to supported  $\text{Ni}/\text{Al}_2\text{O}_3$  catalyst. And the justification for choosing these elements is illustrated in the Section 2.1. A successive impregnation method, as described in our pervious paper, was implemented to synthesize the catalysts [39].

To result into the  $\text{Ni}/\text{Al}_2\text{O}_3$  catalyst with 15 wt% Ni, this typical synthesis procedure was as follows. Initially, the support was added to deionize aqueous solution with appropriate concentration of nickel nitrate hexahydrate with vigorous stirring. The slurry with continuous stirring was then maintained at room temperature overnight. Afterwards, the heating of the solution was controlled at  $80\text{ }^\circ\text{C}$  until the water completely evaporated. Followed by drying process at  $110\text{ }^\circ\text{C}$  in air for 12 h, the mixture finally calcined at  $550\text{ }^\circ\text{C}$  in static air during 4 h at a rate of  $3\text{ }^\circ\text{C min}^{-1}$ .

The  $\text{Ni-X}/\text{Al}_2\text{O}_3$  catalysts ( $X = \text{Na, Ca, Ce, Mg, La, Cu, Zn, Zr, In, Mo, Ti, Pb, Cs, or Bi}$ ) with a  $\text{Ni}/X$  molar ratio of 3 were further obtained utilizing the method mentioned above. Operational details about relevant experimental process are presented by the same authors. Hence, this only gives a brief description of the points that need to be noticed in this process. Two grams of ready-prepared  $\text{Ni}/\text{Al}_2\text{O}_3$  catalyst were required for making up the corresponding aqueous solution. Thereafter, 1.704 mmol of added nitrate reagent was dissolved in the precursor solution to form a suspension. Lastly, through the same rate of heating, a calcination treatment was conducted in a muffle furnace for 4 h at  $450\text{ }^\circ\text{C}$ .

#### 3.3. Catalyst Evaluation

The evaluation of the collected catalysts resistance to sintering for CO methanation reaction was performed at 1 MPa pressure in a fixed bed continuous flow reactor, which made of stainless-steel tubing (i.d. 10mm). About 200 mg of powder catalysts (40–80 mesh), which dispread between quartz wool at the center of the reactor, was reduced at  $500\text{ }^\circ\text{C}$  in a hydrogen flow of  $25\text{ mL min}^{-1}$  for 2 h before starting each experiment and then cooled to the temperature of  $240\text{ }^\circ\text{C}$ . The resulting mixed gas here comprised  $\text{H}_2$  and CO with molar ratio of 3 was then fed into the reactor. The weight hourly space velocity (WHSV) was maintained at  $30,000\text{ mL g}^{-1}\text{ h}^{-1}$ . The temperature range of the measured was between  $240$  and  $800\text{ }^\circ\text{C}$ . The observation points selected are spaced at an interval of  $40\text{ }^\circ\text{C}$ . To evaluate the sintering resistance of the catalyst more effectively, the temperature was kept at  $800\text{ }^\circ\text{C}$  for 24 h. Meanwhile, the outlet gas composition ( $\text{H}_2$ , CO,  $\text{CH}_4$  and  $\text{CO}_2$ ) was analyzed using an online gas chromatograph instrument, which was equipped with thermal conductivity detector (TCD), condensing and separating the generated water before the analysis.

#### 3.4. Structural Characterization

The conventional Ni-based catalysts for this reaction often deactivate severely due to sintering of the Ni particles, which is caused by the poor dispersion of nickel particles because of the weak metal–support interaction between Ni and support [61]. In order to gain an insight into the structure–catalytic anti-sintering properties relationship, powder X-ray diffraction (XRD) characterizations of the catalysts before and after the catalytic reaction were performed in the present study [11].

XRD patterns of the tested samples were obtained in step scanning on a Rigaku D/Max 2500 diffractometer utilizing  $\text{CuK}\alpha$  radiation ( $\lambda = 1.54056\text{ \AA}$ ) operating at 40 kV and 100 mA over a  $2\theta$  range

of 10–80° at 4° min<sup>−1</sup>. The crystallite size characterization of the Ni on the basis of (1, 1, 1) surface was calculated using the following Scherrer–Warren equation [62,63]:

$$d_{(XRD)} = \frac{\kappa\lambda}{\beta\cos\theta}, \quad (2)$$

where  $\kappa$  represents Scherrer's constant, which is 0.94, and  $\lambda$  (incident wavelength) is 1.5418 Å. The half-height width of diffraction peak of the tested sample is described as  $\beta$ . Bragg diffraction angle, which represented as parameter of  $\theta$ , is need to be measured. Here,  $d_{(XRD)}$  only as the descriptor of the crystalline size of perpendicular to the direction of the grain surface has nothing to do with the other directions.

#### 4. Conclusions

In this paper, data-mining technology were successfully developed to the modeling and screening of methanation catalysts. The data mining technology could be conveniently applied to build a new modeling framework and prediction from the high-dimensional, discrete and complex catalytic data arising from catalysis experimentation. The application of regression models within physicochemical properties of elements utilized as promoters of Ni/Al<sub>2</sub>O<sub>3</sub> catalysts has been implemented to predict the resistance to sintering of Ni/Al<sub>2</sub>O<sub>3</sub> catalysts in the field of methanation reactions. A better catalyst, adding Cs into Ni/Al<sub>2</sub>O<sub>3</sub> catalyst, which was discovered by utilizing the regression model with GPR, could obtain excellent anti-sintering catalytic performance. Furthermore, on account of using virtual elements, the influence of physicochemical properties on the anti-sintering was evaluated.

More importantly, the agreement between predicted and observed experiment values was highly acceptable, therefore demonstrating the viability of data-mining techniques in the analysis and prediction of resistance to sintering. This work confirmed that the novel data mining approach with avoiding the huge and blind experimental process may eventually serve as a scientific and efficient tool to optimize the design and screening of new catalytic systems in a more rapid manner.

**Supplementary Materials:** The following are available online at <http://www.mdpi.com/2073-4344/9/6/493/s1>: Content 1: The use of program code in data mining process, Content 2: Explanation of the GPR model reliability, Content 3: XRD characterization of methanation catalysts with different additives before and after the reaction, Files: (a) data.csv (b) pcddata.csv.

**Author Contributions:** The conceptualization of this journal article is from X.H. and J.R.; the experiment was designed by Y.L.; the writing—original draft was prepared by Y.L.; Y.L. and C.Z. contributed in carrying out all experiments and characterization tests as well as analyzing the data; L.Y. helped with the modeling and predicting by using some computer software; J.Z. edited and supervised the paper; J.R. reviewed the manuscript.

**Funding:** This research was funded by the National Natural Science Foundation of China (grant number: 21606159, 21776194 and 21808154) and the Key Research and Development Program of Shanxi Province (grant number: 201703D121022-1 and 201803D121039).

**Acknowledgments:** The authors would like to express their grateful appreciation to Yingchao Dong and Quanxi Xu, who gave us a lot of guidance in the construction of GPR prediction model and the preparation of the software code.

**Conflicts of Interest:** The authors declare no conflict of interest.

#### References

1. Chowdhury, M.B.I.; Hossain, M.M.; Charpentier, P.A. Effect of supercritical water gasification treatment on Ni/La<sub>2</sub>O<sub>3</sub>-Al<sub>2</sub>O<sub>3</sub>-based catalysts. *Appl. Catal. A Gen.* **2011**, *405*, 84–92. [CrossRef]
2. Kopyscinski, J.; Schildhauer, T.J.; Biollaz, S.M.A. Production of synthetic natural gas (SNG) from coal and dry biomass—A technology review from 1950 to 2009. *Fuel* **2010**, *89*, 1763–1783. [CrossRef]
3. Gao, J.; Liu, Q.; Gu, F.; Liu, B.; Zhong, Z.; Su, F. Recent advances in methanation catalysts for the production of synthetic natural gas. *RSC Adv.* **2015**, *5*, 22759–22776. [CrossRef]

4. Zhang, J.; Bai, Y.; Zhang, Q.; Wang, X.; Zhang, T.; Tan, Y.; Han, Y. Low-temperature methanation of syngas in slurry phase over Zr-doped Ni/ $\gamma$ -Al<sub>2</sub>O<sub>3</sub> catalysts prepared using different methods. *Fuel* **2014**, *132*, 211–218. [[CrossRef](#)]
5. Liu, Q.; Tian, Y.; Ai, H. Methanation of carbon monoxide on ordered mesoporous NiO-TiO<sub>2</sub>-Al<sub>2</sub>O<sub>3</sub> composite oxides. *RSC Adv.* **2016**, *6*, 20971–20978. [[CrossRef](#)]
6. Xu, J.; Su, X.; Duan, H.; Hou, B.; Lin, Q.; Liu, X.; Pan, X.; Pei, G.; Geng, H.; Huang, Y.; et al. Influence of pretreatment temperature on catalytic performance of rutile TiO<sub>2</sub>-supported ruthenium catalyst in CO<sub>2</sub> methanation. *J. Catal.* **2016**, *333*, 227–237. [[CrossRef](#)]
7. BP Statistical Review of World Energy 2015. Available online: <http://www.biee.org/meeting-list/bp-statistical-review-world-energy-2015/> (accessed on 27 May 2019).
8. Hu, D.; Gao, J.; Ping, Y.; Jia, L.; Gunawan, P.; Zhong, Z.; Xu, G.; Gu, F.; Su, F. Enhanced Investigation of CO Methanation over Ni/Al<sub>2</sub>O<sub>3</sub> Catalysts for Synthetic Natural Gas Production. *Ind. Eng. Chem. Res.* **2012**, *51*, 4875–4886. [[CrossRef](#)]
9. Hwang, S.; Lee, J.; Hong, U.G.; Jung, J.C.; Koh, D.J.; Lim, H.; Byun, C.; Song, I.K. Hydrogenation of carbon monoxide to methane over mesoporous nickel-M-alumina (M = Fe, Ni, Co, Ce, and La) xerogel catalysts. *J. Ind. Eng. Chem.* **2012**, *18*, 243–248. [[CrossRef](#)]
10. Abdel-Mageed, A.M.; Eckle, S.; Widmann, D.; Behm, R.J. Water assisted dispersion of Ru nanoparticles: The impact of water on the activity and selectivity of supported Ru catalysts during the selective methanation of CO in CO<sub>2</sub>-rich reformat. *J. Catal.* **2016**, *335*, 79–94. [[CrossRef](#)]
11. Liu, Q.; Zhong, Z.; Gu, F.; Wang, X.; Lu, X.; Li, H.; Xu, G.; Su, F. CO methanation on ordered mesoporous Ni-Cr-Al catalysts: Effects of the catalyst structure and Cr promoter on the catalytic properties. *J. Catal.* **2016**, *337*, 221–232. [[CrossRef](#)]
12. Qin, Z.; Ren, J.; Miao, M.; Li, Z.; Lin, J.; Xie, K. The catalytic methanation of coke oven gas over Ni-Ce/Al<sub>2</sub>O<sub>3</sub> catalysts prepared by microwave heating: Effect of amorphous NiO formation. *Appl. Catal. B Environ.* **2015**, *164*, 18–30. [[CrossRef](#)]
13. Gao, J.; Wang, Y.; Ping, Y.; Hu, D.; Xu, G.; Gu, F.; Su, F. A thermodynamic analysis of methanation reactions of carbon oxides for the production of synthetic natural gas. *RSC Adv.* **2012**, *2*, 2358–2368. [[CrossRef](#)]
14. Sabatier, P.; Senderens, J.B. New methane synthesis. *Compt. Rend.* **1902**, *134*, 514–516.
15. Qin, H.; Guo, C.; Wu, Y.; Zhang, J. Effect of La<sub>2</sub>O<sub>3</sub> promoter on NiO/Al<sub>2</sub>O<sub>3</sub> catalyst in CO methanation. *Korean J. Chem. Eng.* **2014**, *31*, 1168–1173. [[CrossRef](#)]
16. Zhang, L.; Gao, Z.; Bao, L.; Ma, H. Influence of the supports ZrO<sub>2</sub> on selective methanation of CO over the nickel supported catalysts. *Int. J. Hydrogen Energy* **2018**, *43*, 9287–9295. [[CrossRef](#)]
17. Guo, C.; Wu, Y.; Qin, H.; Zhang, J. CO methanation over ZrO<sub>2</sub>/Al<sub>2</sub>O<sub>3</sub> supported Ni catalysts: A comprehensive study. *Fuel Proc. Technol.* **2014**, *124*, 61–69. [[CrossRef](#)]
18. Tian, D.; Liu, Z.; Li, D.; Shi, H.; Pan, W.; Cheng, Y. Bimetallic Ni-Fe total-methanation catalyst for the production of substitute natural gas under high pressure. *Fuel* **2013**, *104*, 224–229. [[CrossRef](#)]
19. Rönsch, S.; Schneider, J.; Matthischke, S.; Schlüter, M.; Götz, M.; Lefebvre, J.; Prabhakaran, P.; Bajohr, S. Review on methanation - From fundamentals to current projects. *Fuel* **2016**, *166*, 276–296. [[CrossRef](#)]
20. Konishcheva, M.V.; Potemkin, D.I.; Snytnikov, P.V.; Stonkus, O.A.; Belyaev, V.D.; Sobyenin, V.A. The insights into chlorine doping effect on performance of ceria supported nickel catalysts for selective CO methanation. *Appl. Catal. B Environ.* **2018**, *221*, 413–421. [[CrossRef](#)]
21. Vannice, M.A. The Catalytic Synthesis of Hydrocarbons from Carbon Monoxide and Hydrogen. *Catal. Rev.* **1976**, *14*, 153–191. [[CrossRef](#)]
22. Lim, J.Y.; McGregor, J.; Sederman, A.J.; Dennis, J.S. Kinetic studies of the methanation of CO over a Ni/ $\gamma$ -Al<sub>2</sub>O<sub>3</sub> catalyst using a batch reactor. *Chem. Eng. Sci.* **2016**, *146*, 316–336. [[CrossRef](#)]
23. Yan, X.; Yuan, C.; Bao, J.; Li, S.; Qi, D.; Wang, Q.; Zhao, B.; Hu, T.; Fan, L.; Fan, B.; et al. A Ni-based catalyst with enhanced Ni-support interaction for highly efficient CO methanation. *Catal. Sci. Technol.* **2018**, *8*, 3474–3483. [[CrossRef](#)]
24. Garbarino, G.; Riani, P.; Magistri, L.; Busca, G. A study of the methanation of carbon dioxide on Ni/Al<sub>2</sub>O<sub>3</sub> catalysts at atmospheric pressure. *Int. J. Hydrogen Energy* **2014**, *39*, 11557–11565. [[CrossRef](#)]
25. Wang, X.; Hong, Y.; Shi, H.; Szanyi, J. Kinetic modeling and transient DRIFTS-MS studies of CO<sub>2</sub> methanation over Ru/Al<sub>2</sub>O<sub>3</sub> catalysts. *J. Catal.* **2016**, *343*, 185–195. [[CrossRef](#)]

26. Zhang, G.; Sun, T.; Peng, J.; Wang, S.; Wang, S. A comparison of Ni/SiC and Ni/Al<sub>2</sub>O<sub>3</sub> catalyzed total methanation for production of synthetic natural gas. *Appl. Catal. A Gen.* **2013**, *462–463*, 75–81. [[CrossRef](#)]
27. Nguyen, T.T.M.; Wissing, L.; Skjøth-Rasmussen, M.S. High temperature methanation: Catalyst considerations. *Catal. Today* **2013**, *215*, 233–238. [[CrossRef](#)]
28. Du, J.; Gao, J.; Gu, F.; Zhuang, J.; Lu, B.; Jia, L.; Xu, G.; Liu, Q.; Su, F. A strategy to regenerate coked and sintered Ni/Al<sub>2</sub>O<sub>3</sub> catalyst for methanation reaction. *Int. J. Hydrogen Energy* **2018**, *43*, 20661–20670. [[CrossRef](#)]
29. Bartholomew, C.H.; Pannell, R.B.; Fowler, R.W. Sintering of alumina-supported nickel and nickel bimetallic methanation catalysts in H<sub>2</sub>/H<sub>2</sub>O atmospheres. *J. Catal.* **1983**, *79*, 34–46. [[CrossRef](#)]
30. Kumi, D.O.; Phaahlamohlaka, T.N.; Dlamini, M.W.; Mangezvo, I.T.; Mhlanga, S.D.; Scurrrell, M.S.; Coville, N.J. Effect of a titania covering on CNTs as support for the Ru catalysed selective CO methanation. *Appl. Catal. B Environ.* **2018**, *232*, 492–500. [[CrossRef](#)]
31. Liu, J.; Yu, J.; Su, F.; Xu, G. Intercorrelation of structure and performance of Ni–Mg/Al<sub>2</sub>O<sub>3</sub> catalysts prepared with different methods for syngas methanation. *Catal. Sci. Technol.* **2014**, *4*, 472–481. [[CrossRef](#)]
32. Liu, Q.; Gao, J.; Zhang, M.; Li, H.; Gu, F.; Xu, G.; Zhong, Z.; Su, F. Highly active and stable Ni/γ-Al<sub>2</sub>O<sub>3</sub> catalysts selectively deposited with CeO<sub>2</sub> for CO methanation. *RSC Adv.* **2014**, *4*, 16094. [[CrossRef](#)]
33. Wang, C.; Zhai, P.; Zhang, Z.; Zhou, Y.; Zhang, J.; Zhang, H.; Shi, Z.; Han, R.P.S.; Huang, F.; Ma, D. Nickel catalyst stabilization via graphene encapsulation for enhanced methanation reaction. *J. Catal.* **2016**, *334*, 42–51. [[CrossRef](#)]
34. Gao, L.; Fu, Q.; Wei, M.; Zhu, Y.; Liu, Q.; Crumlin, E.; Liu, Z.; Bao, X. Enhanced nickel-catalyzed methanation confined under hexagonal boron nitride shells. *ACS Catal.* **2016**, *6*, 6814–6822. [[CrossRef](#)]
35. Ding, M.; Tu, J.; Zhang, Q.; Wang, M.; Tsubaki, N.; Wang, T.; Ma, L. Enhancement of methanation of bio-syngas over CeO<sub>2</sub>-modified Ni/Al<sub>2</sub>O<sub>3</sub> catalysts. *Biomass Bioenergy* **2016**, *85*, 12–17. [[CrossRef](#)]
36. Muroyama, H.; Tsuda, Y.; Asakoshi, T.; Masitah, H.; Okanishi, T.; Matsui, T.; Eguchi, K. Carbon dioxide methanation over Ni catalysts supported on various metal oxides. *J. Catal.* **2016**, *343*, 178–184. [[CrossRef](#)]
37. Li, J.; Zhou, L.; Zhu, Q.; Li, H. Enhanced methanation over aerogel NiCo/Al<sub>2</sub>O<sub>3</sub> catalyst in a magnetic fluidized bed. *Ind. Eng. Chem. Res.* **2013**, *52*, 6647–6654. [[CrossRef](#)]
38. Corma, A.; Serra, J.M.; Argente, E.; Botti, V.; Valero, S. Application of artificial neural networks to combinatorial catalysis: Modeling and predicting ODHE catalysts. *ChemPhysChem* **2002**, *3*, 939–945. [[CrossRef](#)]
39. Han, X.; Zhao, C.; Li, H.; Liu, S.; Han, Y.; Zhang, Z.; Ren, J. Using data mining technology in screening potential additives to Ni/Al<sub>2</sub>O<sub>3</sub> catalysts for methanation. *Catal. Sci. Technol.* **2017**, *7*, 6042–6049. [[CrossRef](#)]
40. Gong, D.; Li, S.; Guo, S.; Tang, H.; Wang, H.; Liu, Y. Lanthanum and cerium co-modified Ni/SiO<sub>2</sub> catalyst for CO methanation from syngas. *Appl. Surf. Sci.* **2018**, *434*, 351–364. [[CrossRef](#)]
41. Gao, J.; Xie, C.; Tao, C. Big Data Validation and Quality Assurance—Issues, Challenges, and Needs. *IEEE Symp. Serv. Oriented Syst. Eng. (Sose)* **2016**, 433–441.
42. Omata, K. Screening of new additives of active-carbon-supported heteropoly acid catalyst for Friedel-Crafts reaction by Gaussian process regression. *Ind. Eng. Chem. Res.* **2011**, *50*, 10948–10954. [[CrossRef](#)]
43. Kito, S.; Hattori, T.; Murakami, Y. Determination of synergistically generated acid strength by neural network combined with experiment. *Anal. Sci.* **1991**, *7*, 761–764. [[CrossRef](#)]
44. Omata, K. Screening of supports and additives for heteropoly acid catalyst for Friedel-Crafts reaction by means of high-throughput screening and data mining. *J. Jpn. Petrol. Inst.* **2011**, *54*, 114–118. [[CrossRef](#)]
45. Omata, K. Screening of new additives to heteropoly acid catalyst for Friedel-Crafts reaction by microwave heated HTS and by Gaussian process regression. *Appl. Catal. A Gen.* **2011**, *407*, 112–117. [[CrossRef](#)]
46. Napoleon, D.; Pavalakodi, S. A new method for dimensionality reduction using K-Means clustering algorithm for high dimensional data set. *Int. J. Comput. Appl.* **2011**, *13*, 41–46.
47. Yan, J.; Zhang, B.Y.; Liu, N.; Yan, S.C.; Cheng, Q.S.; Fan, W.G.; Yang, Q.; Xi, W.S.; Chen, Z. Effective and efficient dimensionality reduction for large-scale and streaming data preprocessing. *IEEE Trans. Knowl. Data Eng.* **2006**, *18*, 320–333. [[CrossRef](#)]
48. Eckerson, W.W. *Data Quality and the Bottom Line: Achieving Business Success through a Commitment to High Quality Data*; The Data Warehousing Institute (TDWI): Los Angeles, CA, USA, 2002.
49. Tan, P.; Zhang, C.; Xia, J.; Fang, Q.Y.; Chen, G. NO<sub>x</sub> emission model for coal-fired boilers using principle component analysis and support vector regression. *J. Chem. Eng. Jpn.* **2016**, *49*, 211–216. [[CrossRef](#)]
50. Abdi, H.; Williams, L.J. Principal component analysis. *Wiley Interdiscip. Rev. Comput. Stat.* **2010**, *2*, 433–459. [[CrossRef](#)]

51. Gramacy, R.B. *tgp*: An R Package for Bayesian Nonstationary, Semiparametric Nonlinear Regression and Design by Treed Gaussian Process Models. *J. Stat. Softw.* **2007**, *19*, 1–46. [[CrossRef](#)]
52. Gramacy, R.B.; Taddy, M. Categorical Inputs, Sensitivity Analysis, Optimization and Importance Tempering with *tgp* Version 2, an R Package for Treed Gaussian Process Models. *J. Stat. Softw.* **2010**, *33*, 1–48. [[CrossRef](#)]
53. Niaei, A.; Badiki, T.M.; Nabavi, S.R.; Salari, D.; Izadkhah, B.; Caylak, N. Neuro-genetic aided design of modified H-ZSM-5 catalyst for catalytic conversion of methanol to gasoline range hydrocarbons. *J. Taiwan Inst. Chem. Eng.* **2013**, *44*, 247–256. [[CrossRef](#)]
54. Huang, M.Z.; Han, W.; Wan, J.Q.; Ma, Y.W.; Chen, X.H. Multi-objective optimisation for design and operation of anaerobic digestion using GA-ANN and NSGA-II. *J. Chem. Technol. Biot.* **2016**, *91*, 226–233. [[CrossRef](#)]
55. Adib, H.; Haghbakhsh, R.; Saidi, M.; Takassi, M.A.; Sharifi, F.; Koolivand, M.; Rahimpour, M.R.; Keshtkari, S. Modeling and optimization of Fischer-Tropsch synthesis in the presence of Co (III)/Al<sub>2</sub>O<sub>3</sub> catalyst using artificial neural networks and genetic algorithm. *J. Nat. Gas. Sci. Eng.* **2013**, *10*, 14–24. [[CrossRef](#)]
56. Holena, M.; Linke, D.; Rodemerck, U. Evolutionary optimization of catalysts assisted by neural-network learning. *Lect. Notes. Comput. Sc.* **2010**, *6457*, 220–229.
57. Behler, J. First principles neural network potentials for reactive simulations of large molecular and condensed systems. *Angew. Chem. Int. Edit.* **2017**, *56*, 12828–12840. [[CrossRef](#)] [[PubMed](#)]
58. Yuan, J.; Wang, K.; Yu, T.; Fang, M. Reliable multi-objective optimization of high-speed WEDM process based on Gaussian process regression. *Int. J. Mach. Tool. Manu.* **2008**, *48*, 47–60. [[CrossRef](#)]
59. Pal, M.; Deswal, S. Modelling pile capacity using Gaussian process regression. *Comput. Geotech.* **2010**, *37*, 942–947. [[CrossRef](#)]
60. Jones, D.R.; Schonlau, M.; Welch, W. Efficient global optimization of expensive black-box functions. *J. Glob. Optim.* **1998**, *13*, 455–492. [[CrossRef](#)]
61. Ren, J.; Li, H.; Jin, Y.; Zhu, J.; Liu, S.; Lin, J.; Li, Z. Silica/titania composite-supported Ni catalysts for CO methanation: Effects of Ti species on the activity, anti-sintering, and anti-coking properties. *Appl. Catal. B Environ.* **2017**, *201*, 561–572. [[CrossRef](#)]
62. Lucchini, M.; Testino, A.; Kambolis, A.; Proff, C.; Ludwig, C. Sintering and coking resistant core-shell microporous silica-nickel nanoparticles for CO methanation: Towards advanced catalysts production. *Appl. Catal. B Environ.* **2016**, *182*, 94–101. [[CrossRef](#)]
63. Tada, S.; Kikuchi, R.; Takagaki, A.; Sugawara, T.; Oyama, S.; Urasaki, K.; Satokawa, S. Study of Ru-Ni/TiO<sub>2</sub> catalysts for selective CO methanation. *Appl. Catal. B Environ.* **2013**, *140–141*, 258–264. [[CrossRef](#)]



© 2019 by the authors. Licensee MDPI, Basel, Switzerland. This article is an open access article distributed under the terms and conditions of the Creative Commons Attribution (CC BY) license (<http://creativecommons.org/licenses/by/4.0/>).